AD-A168 885 COMPARISON OF RAYLEIGH-TAYLOR GROWTH WITH 10 MICROMETERS AND 025 MICROMETERS LASERS(U) NAVAL RESEARCH LAB WASHINGTON DC M H EMERY ET AL. 29 MAY 86 NRL-MR-5796 1/1

UNCLASSIFIED F/G 18/1 NL

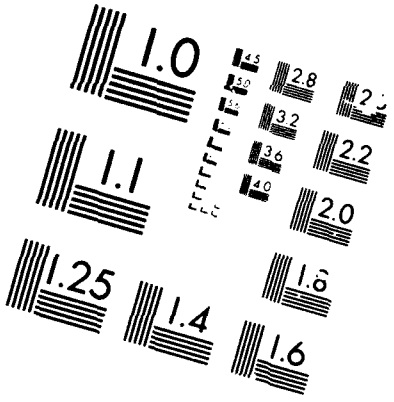
1.0
1.1
1.25
1.4
1.6
2.8
3.2
3.6
4.0
2.2
2.0
1.8

(2)

Comparison of Rayleigh-Taylor Growth with 1.0 μm and 0.25 μm Lasers

M. H. EMERY AND J. H. GARDNER

Laboratory for Computational Physics

S. E. BODNER

Plasma Physics Division

This work was supported by the U.S. Department of Energy and the Office of Naval Research.

SECURITY CLASSIFICATION OF THIS PAGE

REPORT DOCUMENTATION PAGE

1a. REPORT SECURITY CLASSIFICATION UNCLASSIFIED	1b RESTRICTIVE MARKINGS
2a. SECURITY CLASSIFICATION AUTHORITY	3 DISTRIBUTION / AVAILABILITY OF REPORT Approved for public release; distribution unlimited.
2b. DECLASSIFICATION / DOWNGRADING SCHEDULE	
4. PERFORMING ORGANIZATION REPORT NUMBER(S) NRL Memorandum Report 5796	5. MONITORING ORGANIZATION REPORT NUMBER(S)
6a. NAME OF PERFORMING ORGANIZATION Naval Research Laboratory 6b. OFFICE SYMBOL (If applicable) Code 4040	7a. NAME OF MONITORING ORGANIZATION Department of Energy
6c. ADDRESS (City, State, and ZIP Code) Washington, DC 20375-5000	7b. ADDRESS (City, State, and ZIP Code) Washington, DC 20585
8a. NAME OF FUNDING / SPONSORING ORGANIZATION Department of Energy 8b. OFFICE SYMBOL (If applicable)	9. PROCUREMENT INSTRUMENT IDENTIFICATION NUMBER
8c. ADDRESS (City, State, and ZIP Code) Washington, DC 20545	10 SOURCE OF FUNDING NUMBERS PROGRAM ELEMENT NO. / PROJECT NO / TASK NO. 81425 / WORK UNIT ACCESSION NO 44-0859-A-6

11 TITLE (Include Security Classification)

Comparison of Rayleigh-Taylor Growth with 1.0 μm and 0.25 μm Lasers

12 PERSONAL AUTHOR(S)

Emery, M. H., Gardner, J. H. and Bodner, S. E.

13a. TYPE OF REPORT	13b TIME COVERED	14. DATE OF REPORT (Year, Month, Day)	15. PAGE COUNT
Interim	FROM 9/85 TO 3/86	1986 May 29	14

16 SUPPLEMENTARY NOTATION

This work was supported by the U.S. Department of Energy and the Office of Naval Research.

17 COSATI CODES			18. SUBJECT TERMS (Continue on reverse if necessary and identify by block number)
FIELD	GROUP	SUB-GROUP	Rayleigh-Taylor, Numerical simulation, Laser-ablation, Hydrodynamic instability

19 ABSTRACT (Continue on reverse if necessary and identify by block number)

It is shown through numerical simulation, that the Rayleigh-Taylor growth rate in laser-ablatively accelerated targets is reduced below the classical value $(kg)^{1/2}$, by factors of 3-4 with 0.25 μm laser light. The simulation results are supported by an analytical expression for the growth rates. These results provide further evidence for the viability of high-aspect ratio shells in direct-drive laser fusion.

20 DISTRIBUTION / AVAILABILITY OF ABSTRACT	21. ABSTRACT SECURITY CLASSIFICATION	
☒ UNCLASSIFIED/UNLIMITED ☐ SAME AS RPT. ☐ DTIC USERS	UNCLASSIFIED	
22a NAME OF RESPONSIBLE INDIVIDUAL Mark H. Emery	22b TELEPHONE (Include Area Code) (202) 767-3196	22c. OFFICE SYMBOL Code 4040

DD FORM 1473, 84 MAR 83 APR edition may be used until exhausted
All other editions are obsolete

SECURITY CLASSIFICATION OF THIS PAGE

COMPARISON OF RAYLEIGH-TAYLOR GROWTH WITH 1.0 μm AND 0.25 μm LASERS

One of the most critical issues facing direct drive laser fusion is that of hydrodynamic stability. In laser fusion a pellet is imploded by ablating material from the outer surface. The acceleration of a cold, dense shell by a hot, light blowoff plasma is an unstable arrangement. The Rayleigh-Taylor (RT)[1], or interchange, instability transposes the position of the more dense fluid with the fluid of lower density in order to reach a more stable configuration. This instability is a potential obstacle to laser fusion since it can cause shell fracture, fuel mix or, in its mildest form, a nonuniform implosion that will reduce the convergence and severely diminish the energy gain of the fusion pellet.

Perhaps the most serious implication of the RT instability is that it ultimately dictates the allowed aspect ratio $R/\Delta R$ (ratio of the distance pushed to the shell thickness) for the shell. The allowed aspect ratio both fixes the pressure required to drive the shell inward and indirectly determines the efficiency of the energy coupling between the laser and the shell[2]. If the RT grows at its classically predicted rate, then thick, low-aspect ratio shells must be used. This, in turn, implies laser intensities at or above the threshold for plasma instabilities and unacceptably low rocket efficiencies.

The allowed aspect ratio for the laser-ablative case is a function of the RT growth rate and the wavelength of the most dangerous mode. Classical theory[1] predicts that an initial perturbation, η_o, on the interface of an unstably stratified fluid in planar geometry will grow as $\eta(t) = \eta_o e^{\gamma t}$, where $\gamma = (A\ kg)^{1/2}$, $k = 2\pi/\lambda$, where λ is the wavelength of the perturbation, g is the acceleration, $A = (\rho_h - \rho_\ell)/(\rho_h + \rho_\ell)$ is the Atwood number and $\rho_h(\rho_\ell)$ is the density of the heavy (light) fluid. ($A \sim 0(1)$ in the laser-ablative case.) If the perturbation wavelength is much smaller than the radius (R_o) of a spherical pellet, then the planar growth rate can be applied, at a first approximation, to spherical geometry. Let us assume that the growth rate for the laser-ablative case is $\varepsilon(kg)^{1/2}$, where $\varepsilon < 1$. If the shell is imploded at constant acceleration half-way inward, a good approximation to present designs, then the number of e-foldings of unstable growth is $\gamma t = \varepsilon(2\pi R_o/\lambda)^{1/2}$. Classical, incompressible theory suggests that the most dangerous mode is $\lambda = \Delta R$, the thickness of the shell, as then,

Manuscript approved March 10, 1986.

the inner and outer surfaces are strongly coupled. However, numerical simulations have shown that when compressibility and nonlinear effects are taken into account, it is those perturbation wavelengths several, O(3), times the shell thickness which are most damaging to the implosion process[3]. For mathematical convenience, we set $\lambda = \pi\Delta R$, and the limiting aspect ratio is given by $R_o/\Delta R = 1/2(\frac{\pi t}{\epsilon})^2$.

This limit is quite severe since an initial aspect ratio of 10 or so can become an in-flight-aspect-ratio (IFAR) of $\sim$ 150 as a result of compression due to the 20-40 Mb ablation pressure. Consider a pellet polished so that after compression the largest surface perturbation has an amplitude of $\sim 100\mathring{A}$ and assume that the implosion process can survive 6 e-foldings of RT growth. If the RT grows at its classical rate ($\epsilon = 1$) then the maximum IFAR is limited to a value less than 20. The initial aspect ratio for this pellet would be about 1.5 . The laser intensity required to generate sufficient pressure to accelerate this shell to implosion velocities would be well above the threshhold for plasma instabilities. These thick low-aspect ratio shells would also severely limit the efficiency and gain of a fusion pellet[4].

Both numerical simulations[5] and experiments[6] at 1μm laser light indicate that the RT growth rate in the laser-ablative case is about 1/2 of the classically predicted value ($\epsilon = 1/2$). This would allow an IFAR $\sim$ 70, which is marginal at best. Unless the RT growth rate is reduced even further than that obtained with 1μm laser light, these thin, high-aspect ratio shells will rupture well before the fuel compression stage. It is this enhanced reduction in the growth rate at shorter laser wavelengths we wish to discuss in this letter.

The RT instability is modeled using the FAST2D laser-shell simulation code. This is a fully two-dimensional Cartesian code with a sliding Eulerian grid with variable grid spacing. The grid spacing is 0.25μm for 15 zones on either side of the ablation layer and increases uniformly to 2 μm for most of the rest of the grid. The refined subzoning follows the ablation front throughout the course of the run. FAST2D solves the ideal hydrodynamic equations using the flux-corrected-transport algorithms with two-dimensional classical ($T^{5/2}$) plasma thermal conduction. The code has been extensively documented against experimental data[3,7] and is discussed in some detail in Ref. 7 and references therein. The initial steady state density profile is perturbed at its peak

with a single sinusoidal mode corresponding to a total initial mass perturbation of less than 0.5%. The laser pulse has a 2 ns Gaussian rise after which the laser intensity is held constant. The computational growth rates are obtained by Fourier transforming the summed mass of the foil which is integrated from the rear of the foil to the ablation edge for each transverse coordinate. The growth rate is measured during the constant phase of the laser pulse. Typically 6-7 e-foldings of exponential growth are obtained.

Figure 1 compares the growth rate obtained from the FAST2D simulation (—— • ——) to $(kg)^{1/2}$ (——) for 1μm laser light with an absorbed intensity of $10^{13}\ W/cm^2$ impinging a 20μm thick plastic (CH) target. The computational growth rates have a $k^{1/2}$ dependence with a moderately strong cutoff for the short wavelength modes. The computational growth rates are about a factor of 1.5 - 2 less than the classically predicted value.

The inhibited nature of the RT growth rate for the laser-ablative case is even more apparent for shorter wavelength lasers. For this case, the laser intensity was increased to a value closer to fusion conditions. Figure 2 compares the FAST2D simulation results (—— • ——) to $(kg)^{1/2}$ (—) for $1/4\mu$m laser light with an absorbed laser intensity of $3 \times 10^{14} W/cm^2$. The target is a 20μm thick plastic (CH) foil. The numerical growth rates for this case are a factor of 3-4 less than the classically predicted values. The ratio of the numerical growth rate to $(kg)^{1/2}$ for both the 1μm results (•, from Fig. 1) and the $1/4\mu$m results (x, from Fig. 2) is plotted as a function of perturbation wavelength in Figure 3. Note that for wavelength perturbations of $O(60\mu m)$, three times the foil thickness, the growth rate has been reduced by a factor of 1.8 for 1μm lasers and by a factor of 3.5 for $1/4\mu$m lasers.

The strong dependence of growth rate upon the laser wavelength can be understood in terms of the mechanism that we believe is responsible for the reduction below the classical value : the ablative convection of the vorticity away from the unstable ablation surface[8]. It is the vorticity generated at the unstable interface which controls the interchange of the two fluids. As a result of the laser-ablative process, part of that vorticity is convected away thereby reducing the growth rate of the instability. If the ablation velocity (V_a) is included in the two-dimensional vorticity equation through the convective term, the growth rate for the RT instability in a laser ablatively-accelerated

target is given by[9]

$$\gamma = [(kV_a/2)^2 + \gamma_o^2]^{1/2} - kV_a/2 \quad (1)$$

where $\gamma_o = (kg)^{1/2}$, the classical growth rate. When the ablation velocity is large, then the classical RT growth rate is strongly reduced. The above expression (x) is compared to the FAST2D simulation results (•) in Figures 1 and 2. The agreement is quite good for both the 1μm and the $1/4\mu$m cases. The ablation velocities are taken from the numerical simulations and are measured at the center of the unstable shear layer on the ablation front. See Figure 4. The ablation velocities have the values of 1.3×10^6 cm/s for the 1μm case, at $10^{13}W/cm^2$, and 5.5×10^6 cm/s for the $1/4\mu$m case, at $3 \times 10^{14}W/cm^2$. The lack of agreement at the short wavelength perturbations for the 1μm case is due to the assumption of an infinitely thin vortex sheet at the ablation layer. If γ_o in Eq. 1 is replaced by the growth rate for an exponential density layer of finite thickness, then the cutoff is reproduced[9].

The strongly inhibited growth for $1/4\mu$m lasers is due to a very large ablation velocity. Shorter wavelength lasers deposit their energy closer to the ablation front and produce a higher mass ablation rate. This higher mass ablation rate produces a higher acceleration of plasma away from the target surface, and therefore a larger value of V_a. Figure 5 is a plot of the ablation velocity (V_a) obtained from the FAST2D simulation model as a function of the distance from the target surface for three laser wavelengths (1, 1/2 and 1/4 μm). All the calculations were with a 20μm thick CH foil with approximately the same isentrope with an absorbed laser intensity of $5 \times 10^{13}W/cm^2$. Note that at a distance of $\frac{3}{4}\mu$m from the target surface, which is at the center of the unstable shear layer, the ablation velocity for $1/4\mu$m light is over three times larger than for 1μm light.

This result can be seen more clearly from a scaling arguement. The expansion velocity measured near critical scales as $V_c \propto (I\lambda_\ell^2)^{1/3}$ and the ablation pressure scales as $P_a \propto (I/\lambda_\ell)^{2/3}$ in planar geometry[10]. I is the laser intensity and λ_ℓ is the laser wavelength. This scaling is somewhat different for spherical geometry ($P_a \propto (I/\lambda_\ell^{1/4})^{2/3}$) [11] but the argument still holds. From the conservation of mass $\rho_a V_a = \rho_c V_c$ where

$\rho_a(V_a)$ is the density (velocity) to be determined very near the ablation layer. Assume that the target and laser profiles can be designed so that the targets are on the same isentrope; i.e., $P_a/\rho_a^{5/3}$ = constant, irrespective of laser intensity and wavelength. If the ablation pressure is kept constant as the laser wavelength is reduced then $I \ \alpha\lambda_\ell$ and the ablation velocity scales as $V_a \ \alpha \ \lambda_\ell^{-1}$. If the ablation pressure is allowed to vary then $V_a \ \alpha \ \lambda_\ell^{-14/15}$. Thus, although the blowoff velocity at critical decreases with decreasing laser wavelength, the ablation velocity measured near the target surface increases with decreasing laser wavelength. Note that the target acceleration ($g = P_a/M, M$ is the target mass) is constant if the ablation pressure is held fixed and scales as $g \ \alpha \ \lambda_\ell^{-2/3}$ if P_a is allowed to vary with laser wavelength. The scaling for the ablation velocity is a stronger function of laser wavelength. The growth rate for the RT instability will then be more strongly inhibited with short wavelength lasers than with 1μm laser light, since the vorticity will be convected away at a faster rate, see Eq. 1.

We have shown that the RT growth rate for laser ablatively-accelerated targets is strongly reduced below the classically predicted value for short wavelength lasers. By combining the most damaging perturbation wavelength of $O(60\mu m)$, about 3 times the shell thickness, with a growth rate that is 3.5 times smaller than the classical value, $\varepsilon \approx 1/3.5$, and up to 6 e-foldings of exponential growth, we conclude that the maximum IFAR for a reactor-sized pellet driven with 1/4μm laser light is $R/\Delta R \approx$ 220. If one designs for a direct illumination pellet with an IFAR of order 150 using 1/4μm light, then the net (rocket times absorption) efficiency can be as high as 10%[4]. Pellet gains can then be on the order of 200 - 300, or even higher, depending on other physics constraints[2]. This suggests that high-aspect ratio shells are indeed a viable and highly attractive design for direct-drive laser fusion. Clearly, we now need additional experimental data on the RT instability under various conditions to test these predictions. We thank P. C. Reed for her technical assistance. This work was supported by the U. S. Department of Energy and the Office of Naval Research.

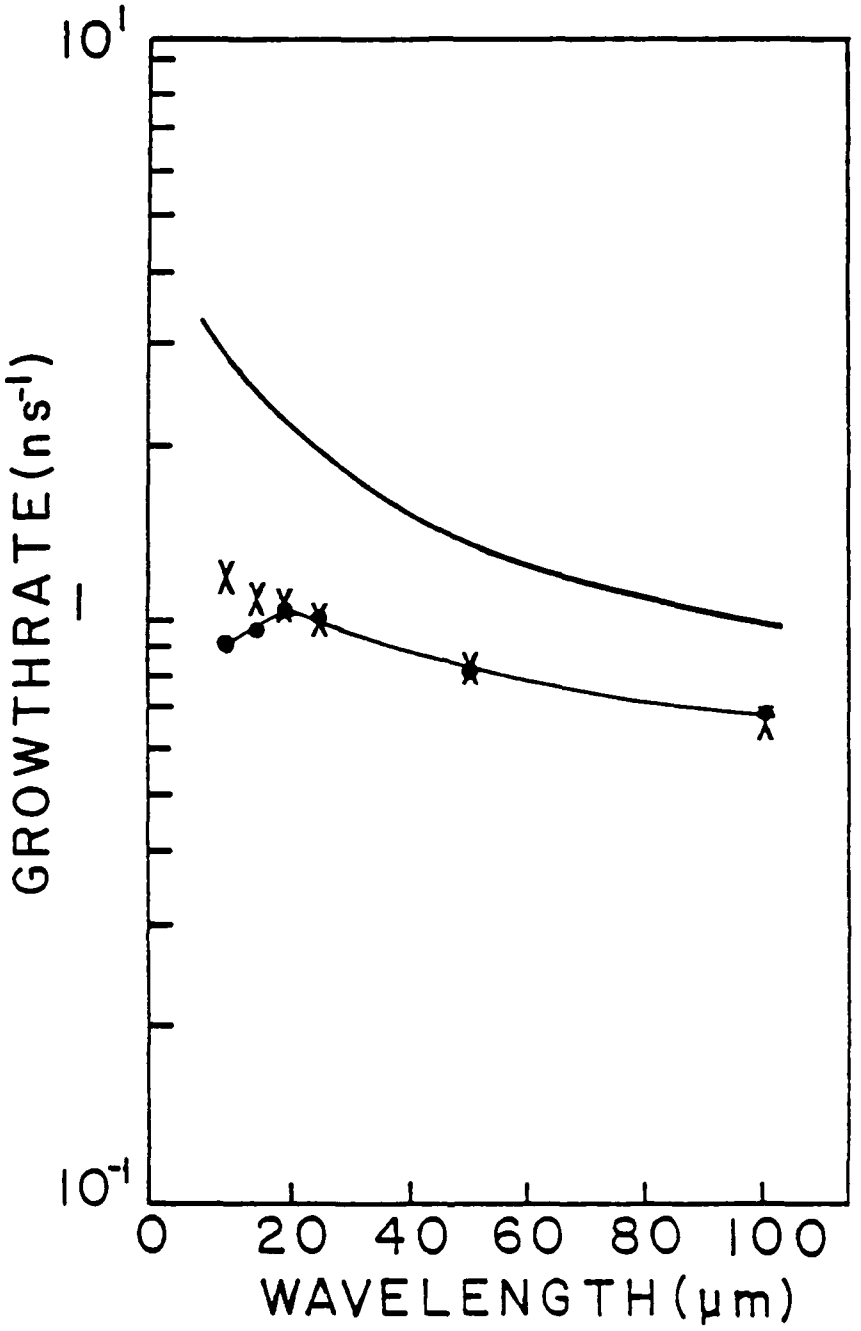

Figure 1. Comparison of the classical growth rate ($(kg)^{1/2}$,—) to the simulation results ($\cdot$) and to the theoretical result (Eq. 1, x) for 1μm laser light with an absorbed intensity of 10^{13} W/cm^2 impinging 20μm thick plastic (CH) foils. The ablation velocity is measured at the center of the shear layer, $0(1\mu m)$ from the target surface, and is the same for all perturbation wavelengths, $V_1 = 1.3 \times 10^6 cm/s$.

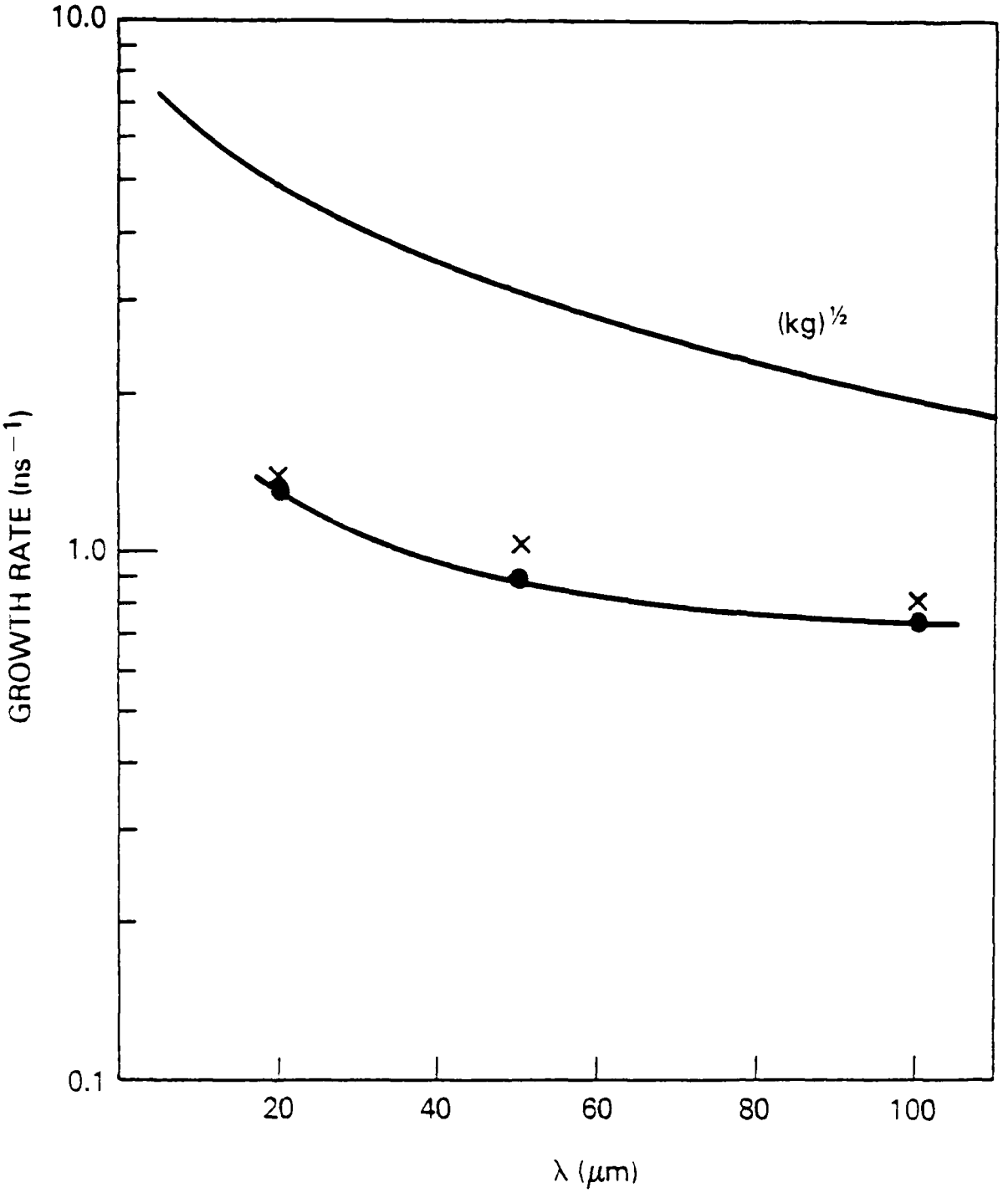

Figure 2. Comparison of the simulation results (·) to the classical growth rate (—) and to the theoretical prediction (x) for $\frac{1}{4}\mu$m laser light with an absorbed intensity of $3 \times 10^{14} W/cm^2$.

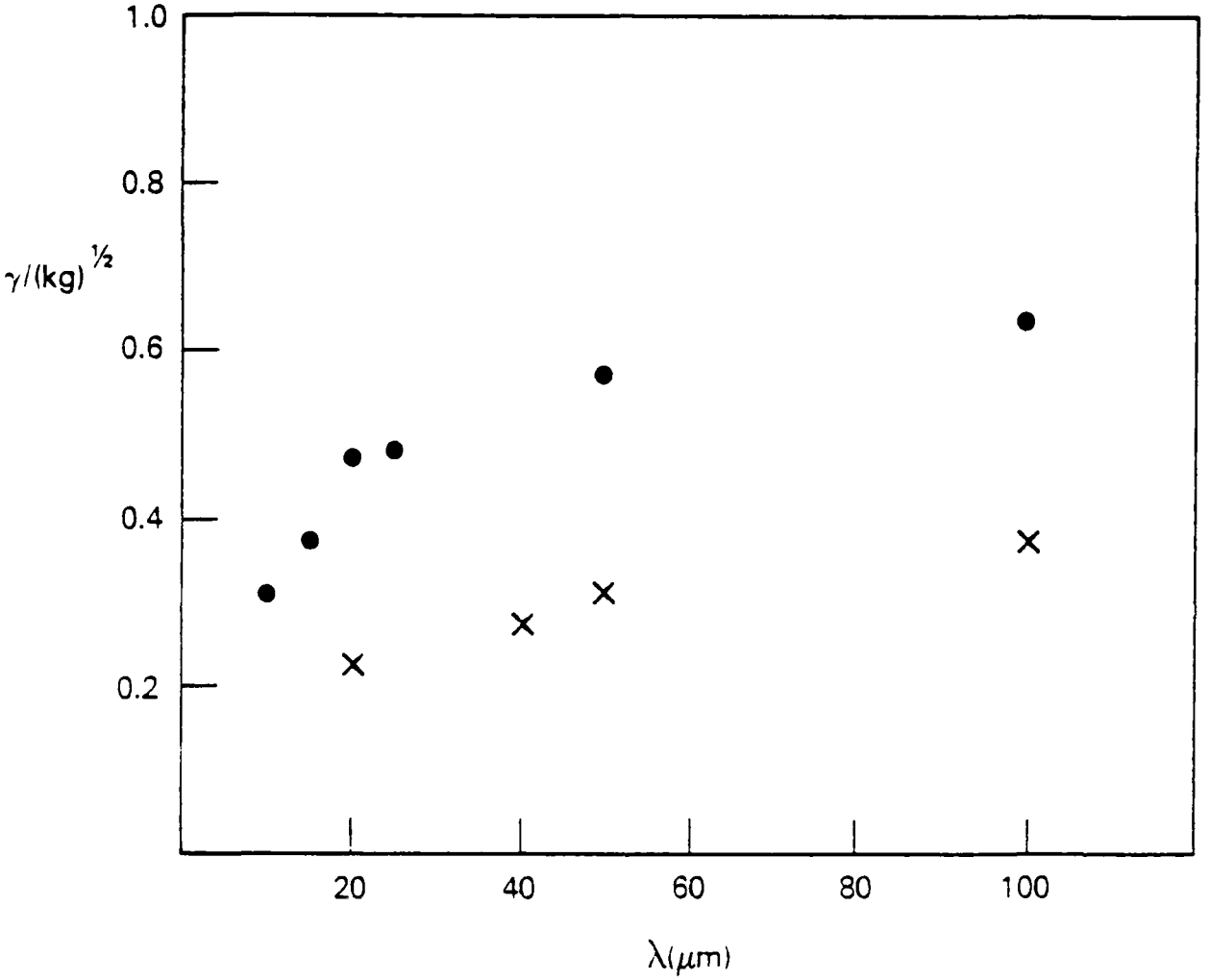

Figure 3. Plot of the ratio of the numerical growth rate to $(\mathrm{kg})^{1/2}$ for 1μm (·) and $\frac{1}{4}\mu$m (x) laser light is with an absorbed intensity of 10^{14} W/cm^2.

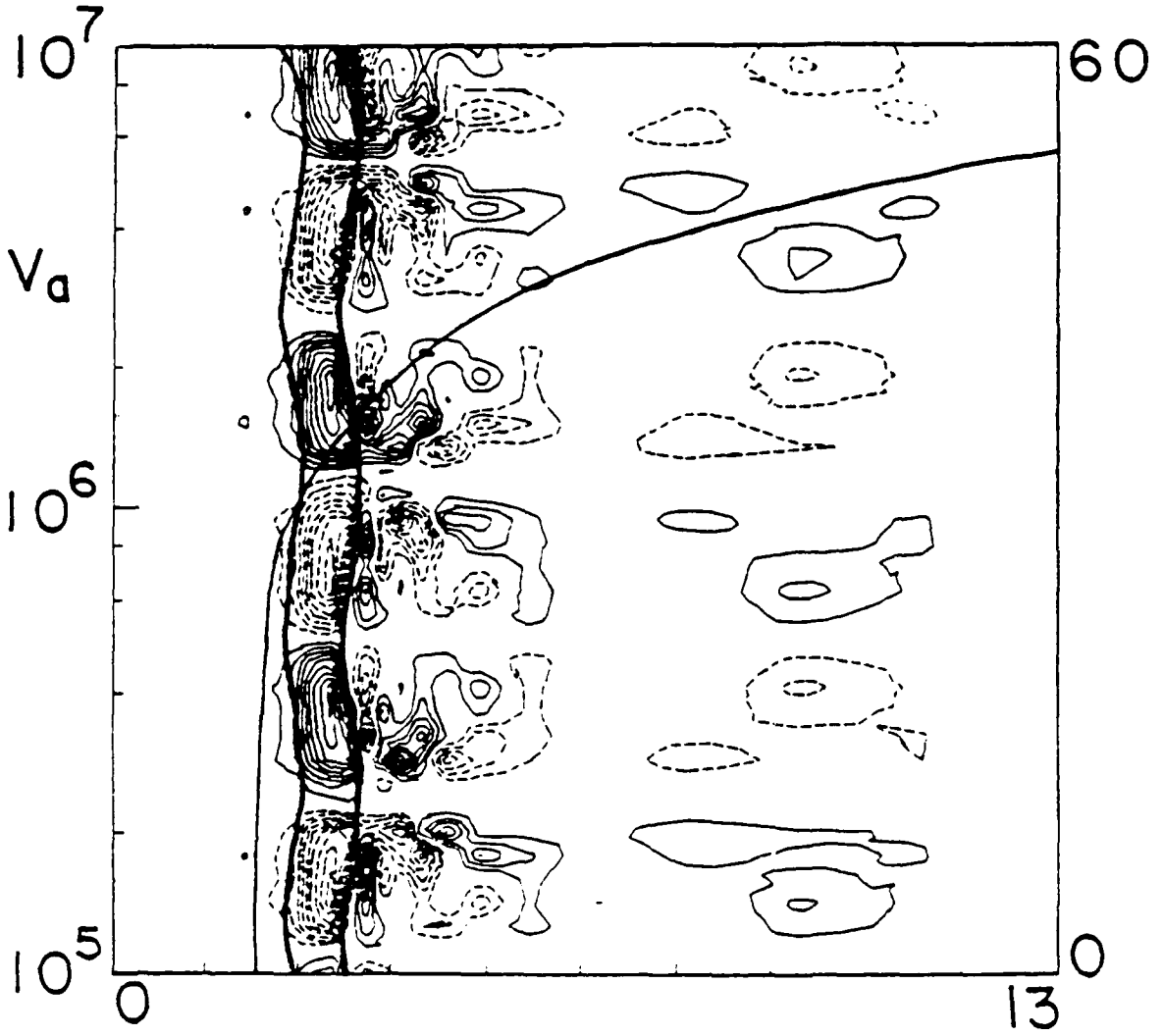

Figure 4. Isovorticity contours, in 10 % increments of the maximum, on the target surface early in the evolution of the 20μm RT instability for the 1μm laser case. The laser is impinging the target from the right. The spatial dimensions are in μm. The dashed (solid) contours indicate clockwise (counter clockwise) flow. The wavy bold lines delineate the 10 % (right) and 80 % (left) density contours. The ablation velocity ($V_a, cm/s$), which is convecting vorticity away from the target surface, is plotted on top of the vorticity contours. The value of V_a at the center of the layer is $1.3 \times 10^6 cm/s$.

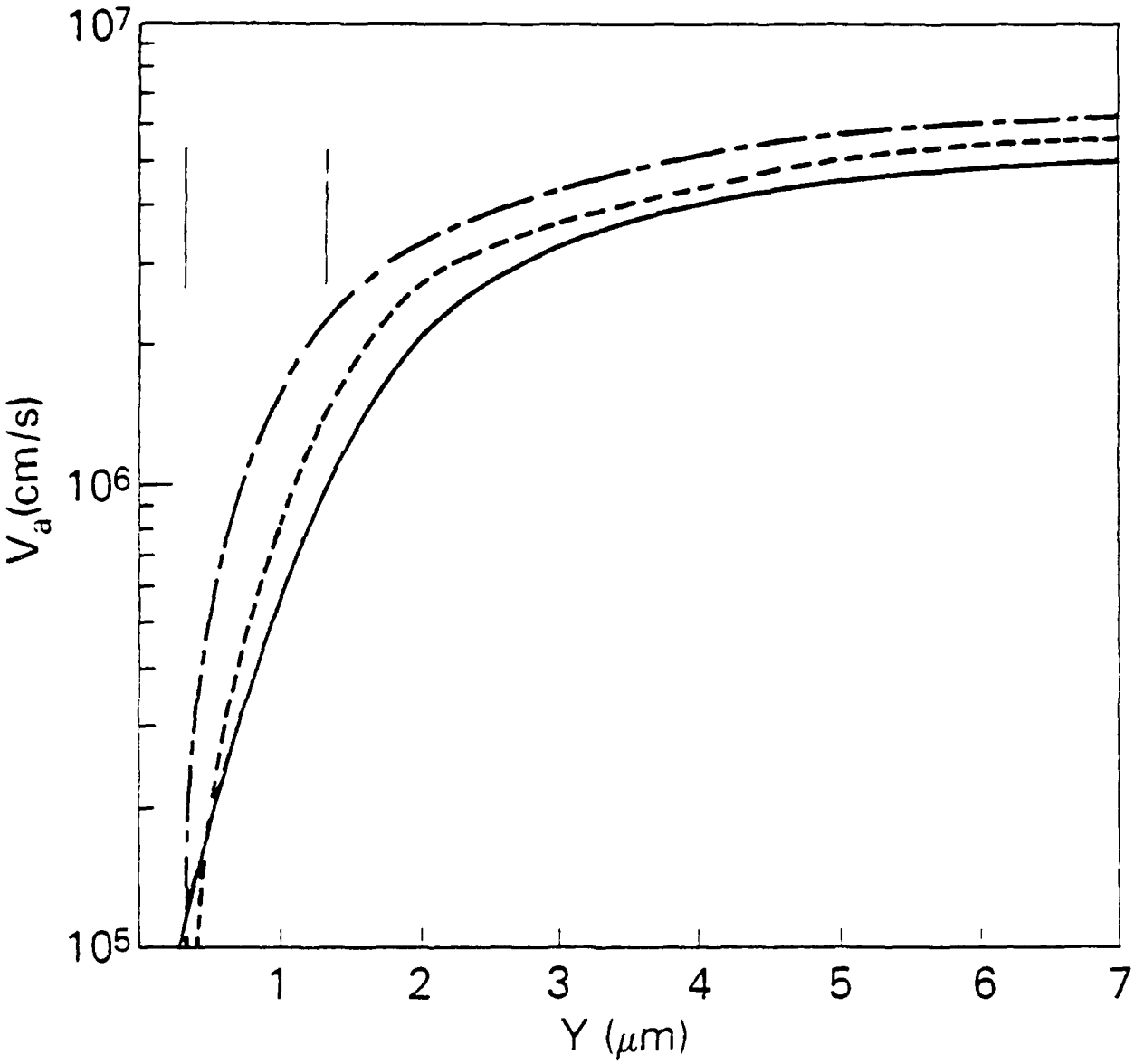

Figure 5. Plot of the ablation velocity (V_a) as a function of distance from the target surface (Y) for 1μm (solid), $\frac{1}{2}\mu$m (dash) and $\frac{1}{4}\mu$m (dash-dot) laser light at $5 \times 10^{13} W/cm^2$ impinging a flat 20μm thick plastic (CH) foil. The curves begin to cross at distances $0(40\mu m)$ from the target surface. The vertical lines bracket the vortex layer (see Ref. 3).

References

1. Lord Rayleigh, Theory of Sound (Dover Publications, Inc., New York (1894), 2nd ed., Vol. 2; G.I. Taylor, Proc. Roy. Soc. (London) A201. 192 (1950).

2. S.E. Bodner, J. Fus. Energy 1 221 (1981).

3. M.H. Emery et al., Appl. Phys. Lett. 41, 808 (1982).

4. J.H. Gardner and S.E. Bodner, Bull. Am. Phys. Soc. 29, 1290 (1984); S.E. Bodner et al., Plasma Phys. and Cont. Nuc. Fus. Res. 3, 155 (1984).

5. C.P. Verdon et al., Phys. Fluids 25, 1653 (1982); M.H. Emery et al., Phys. Rev. Lett. 48, 677 (1982).

6. R.R. Whitlock et al., Phys. Rev. Lett. 52, 819 (1984); J. Grun et al., Phys. Rev. Lett. 53, 1352 (1984).

7. M.H. Emery et al. Phys. Rev. Lett. 48, 253 (1982); P.G. Burkhalter et al., Phys. Fluids 26, 3650 (1983); M.J. Herbst et al., Phys. Rev. Lett. 52, 192 (1984).

8. M.H. Emery et al., Phys. Fluids 27, 1338 (1984).

9. M.H. Emery, Bull. Am. Phys. Soc., Invited paper 3A5, 29, 1231 (1984); to be submitted to Phys. Fluids.

10. W.M. Manheimer and D.G. Colombant, Phys. Fluids 27, 983 (1984).

11. J.H. Gardner and S.E. Bodner Phys. Rev. Lett. 47, 1137 (1981).

END

DTIC

8-86